Quantitative infrared photothermal microscopy

Ilia M. Pavlovetc[a,*], Eduard A. Podshivaylov[b], Pavel A. Frantsuzov[c], Gregory V. Hartland[a], and Masaru Kuno[a,d,*]

[a]Department of Chemistry and Biochemistry, University of Notre Dame, Notre Dame, IN 46556,USA

[b]Lomonosov Moscow State University, 119991 Moscow, Russia

[c]Voevodsky Institute of Chemical Kinetics and Combustion SB RAS, 630090 Novosibirsk,Russia

[d]Department of Physics, University of Notre Dame, Notre Dame, IN 46556, USA

ABSTRACT

Infrared photothermal heterodyne imaging (IR-PHI) represents a convenient table top approach for conducting superresolution imaging and spectroscopy throughout the all-important mid infrared (MIR) spectral region. Although IR-PHI provides label-free, superresolution MIR absorption information, it is not quantitative. In this study, we establish quantitative relationships between observed IR-PHI signals and relevant photothermal parameters of investigated specimens. Specifically, we conduct a size series analysis of different radii polystyrene (PS) beads so as to quantitatively link IR-PHI signal contrast to specimen heat capacity, MIR peak absorption cross-section, and scattering cross-section at IR-PHI's probe wavelength.

Keywords: Photothermal imaging, Infrared spectroscopy, Mid infrared, Infrared Microscopy, Super-resolution imaging

1. INTRODUCTION

The study of light-matter interactions is one of the most powerful means to understanding the physical and chemical properties of materials. Advances in nanoscience require the ability to observe and investigate chemical interactions at the single particle or even single molecule level. Here, Moerner and Kador's seminal work on single molecule detection[1] has paved the way to optical techniques suitable for detecting single analyte species. These approaches are largely emission-based since they are intrinsically low background measurements simple to implement and perform.[2,3] Despite their strengths, however, emission-based methods lack universality since they cannot be used to detect non-emissive species.

In contrast, absorption/extinction-based approaches are general and widely applicable. Several techniques have therefore been developed in the past decade to probe the absorption of single particles.[4] These include direct approaches such as frequency-,[1,5] polarization-,[6] intensity-,,[7] and spatial-modulation,[8,9] absorption microscopies. They also include indirect methods such as photothermal heterodyne imaging (PHI).[10–13]

Among techniques, PHI is the most popular single particle absorption microscopy used today. Its operating principle is based on the well known photothermal effect[14] wherein change to sample optical properties follow the resonant absorption of (pump) light. These changes, directly linked to the absorption of pump light, are detected using a second (probe) beam. By modulating the excitation source, induced changes modulate at the same frequency and facilitate subsequent use of lock-in amplifiers for sensitive signal extraction.

*Further author information: (Send correspondence to I.M.P. or M.K.)

I.M.P.: E-mail: ipavlove@nd.edu

M.K.: E-mail: mkuno@nd.edu

Notably, PHI has been used to detect a single molecule with an absorption cross section of $\sigma_{abs} \sim 5 \times 10^{-16}$ cm^2.[15] An important disadvantage of PHI, though, is that, generally speaking, PHI signal contrast is not a quantitative measure of absorbed light (i.e. it does not immediately yield absolute specimen cross sections or absorption efficiencies). This issue has been overcome by direct comparison of PHI signal amplitudes to those of systems having known absorption efficiencies. This feature has been exploited to measure the size-dependent absorption cross section of individual CdSe nanowires though comparison to PHI signals of gold nanoparticles with known (Mie theory) cross sections.[13]

At the same time, single particle detection, whether emission or absorption-based is rare in the infrared (IR).[16–20] MIR techniques that do exist are mostly scanning probe-based that exploit either photothermal or near-field scattering enhancements to sample extinction. All, however, suffer from instrumental complexity, slow scan speeds, limited fields of view, and complex sample preparation requirements. This, despite possessing impressive spatial resolutions on the order of ~ 20 nm.

IR photothermal heterodyne imaging (IR-PHI)[21–30] is an emerging, all-optical technique to conduct single particle MIR absorption measurements. The technique is far-field in nature and has a demonstrated spatial resolution of order 300 nm.[26] Its operating principle is near identical to that involved in PHI with the primary difference being the use of a MIR pump laser to excite analyte specimens. An additional difference is the general absence of a photothermal medium surrounding the specimen.[22,24–28] This is to avoid potential competing molecular resonances. Compared to abovementioned scanning probe techniques, IR-PHI represents a simple, tabletop approach for the MIR characterization of individual nanostructures.

In what follows, we establish a better understanding of IR-PHI's signal generation mechanism, making essential steps towards revealing quantitative relationships that exist between the IR-PHI signal contrast and specimen physical properties. This is made possible through a series of size-dependent measurements, conducted on different radii polystyrene (PS) beads ($r = 100, 230, 300, 400, 550$ nm) with absorption efficiencies known *a priori* using Mie theory.

2. EXPERIMENTAL

Figure 1 first illustrates the IR-PHI instrument arranged in a counter-propagating pump/probe geometry.[26] The instrument consists of a tunable, pulsed ($\lambda = 2.5 - 3.7\mu$m, $k = 2670 - 4000$ cm^{-1}) MIR optical parametric oscillator (M Squared Lasers, OPO) for the pump and a continuous wave (CW), 532 nm, DPSS laser for the probe. Samples on CaF_2 coverslips (Crystran) are raster scanned through the pump and probe focii using a closed-loop nano-positioning piezo stage (Mad City Labs). The OPO output is focused through the coverslip onto the sample using a 0.65 NA *reflective* objective (Ealing) while the probe laser is focused onto the same spatial position using a 0.95 NA *refractive* objective (Nikon). Substrate-reflected and photothermally-modulated probe light are then collected with the *refractive* objective and are directed onto a photodiode. Heterodyning of these components at the detector then gives rise to a signal modulation at the IR pump repetition rate. The IR-PHI signal is demodulated via lock-in (Stanford Research Systems, SRS 844) detection referenced to the OPO repetition rate. **Figure1** illustrates the employed setup.

IR-PHI samples consist of different radii (r) polystyrene (PS, Sigma Aldrich) bead suspension ($r = 100, 230, 300, 400, 550$ nm) drop cast onto a methanol-cleaned and flamed/plasma cleaned CaF_2 coverslips. Corresponding absorption cross-sections (σ_{abs}) at 3030 cm^{-1} (CH_2 stretch) are estimated using the Mie theory and range from 3.4×10^{-12} to 7.5×10^{-11} cm^2.

3. RESULTS AND DISCUSSION

Figure 2a illustrates IR-PHI imaging results of single $r = 100$ nm PS particles. The pump laser is tuned to $\lambda = 3300$ nm (3030 cm^{-1}), which corresponds to PS's CH_2 resonance. The corresponding peak IR absorption

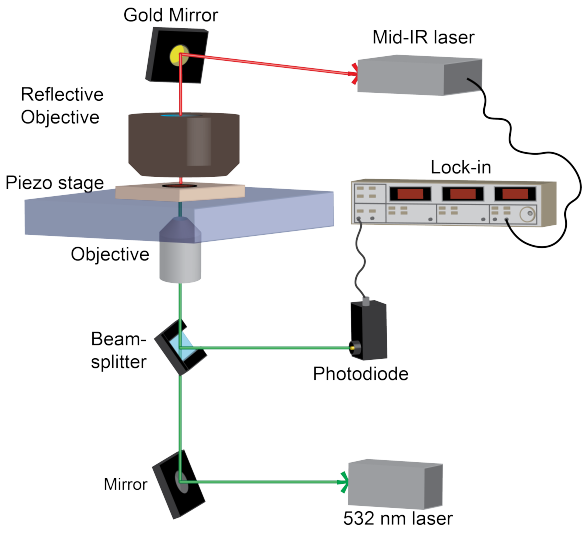

Figure 1: Schematic representation of the IR-PHI setup

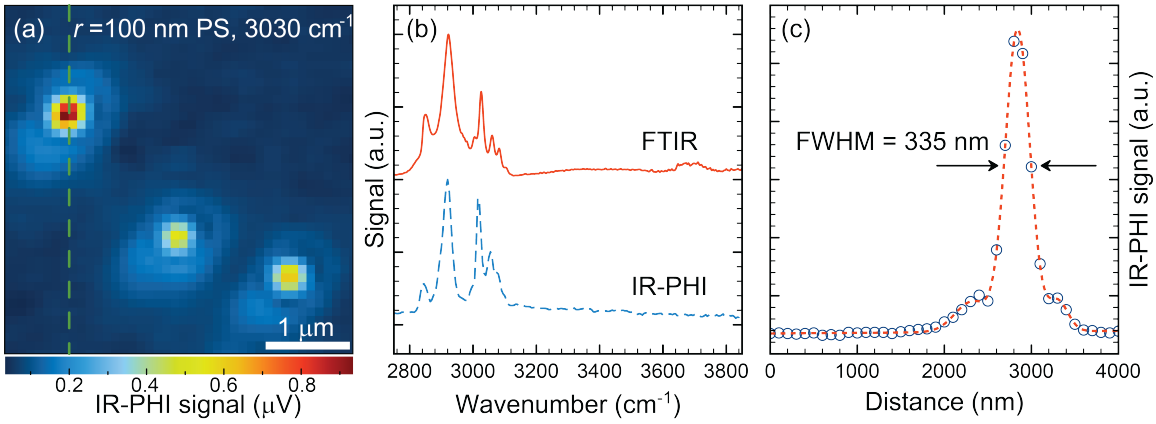

Figure 2: (a) IR-PHI image of three single $r = 100$ nm PS particles acquired at 3030 cm^{-1}. (b) Corresponding single particle PS spectrum compared to the bulk PS FTIR spectrum. (c) Line profile of a particle in panel (a).

cross-section at this wavelength is $\sigma_{\text{abs}} = 3.4 \times 10^{-12}$ cm^2. **Figure 2b** shows an associated single PS particle IR-PHI spectrum along the bulk PS Fourier Transform Infrared (FTIR) spectrum. The excellent agreement between spectra shows spectral fidelity of the technique. **Figure 2**c) shows the line profile through a single bead image in **Figure 2a**. An associated full width at half maximum (FWHM) is 335 nm, which is more than an order of magnitude smaller than corresponding FWHM of the incident IR pump light.

To understand IR-PHI signal contrast, we first assume that it is photothermal in nature. The IR-PHI signal amplitude (P_{PHI}) is consequently proportional to the instantaneous temperature jump (ΔT) induced in the specimen through the absorption of pump light (i.e. $P_{\text{PHI}} \propto \Delta T$). From the definition of heat capacity,[31] a corresponding specimen temperature change is therefore:

$$\Delta T = \frac{P_{\text{abs}}}{C} = \frac{I_{\text{exc}}\sigma_{\text{abs}}}{C} \tag{1}$$

where P_{abs} is the absorbed pump power, C is the sample's heat capacity, and I_{exc} (σ_{abs}) is the pump intensity

(specimen peak absorption cross-section). Of note, is that σ_{abs} exhibits a r^3 size dependency suggesting nonlinear growth of P_{PHI}. However, C also scales with particle volume such that ΔT is only expected to grow 1.7 times between $r = 100$ and $r = 550$ nm. Estimated instantaneous ΔT values therefore range from 34.5 ($r = 100$ nm) to 53.4 K ($r = 550$ nm).

Figure 3 now shows acquired IR-PHI data, which reveals P_{PHI} to increase linearly with size as suggested by **Equation 1**. However, the IR-PHI signal increases from $\sim$ 200 nV to $\sim$ 5 μV, which exceeds the expected 1.7x change by over an order of magnitude. This suggests that that ΔT alone cannot be the sole contributor to IR-PHI optical contrast.

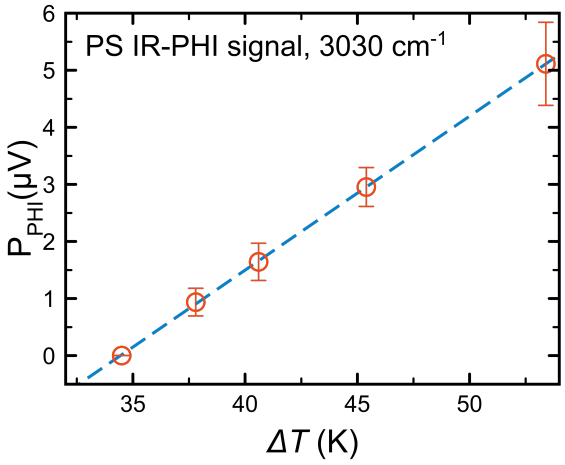

Figure 3: IR-PHI signal size and ΔT dependency. Circles denote experimental IR-PHI values. The dashed line is a fit through the data points.

Here, Hartland[26] has previously suggested, using Finite Element simulations, that temperature-induced changes to scattering cross-sections ($\Delta\sigma_{\text{scat}}$) play an important role in establishing IR-PHI signal contrast (i.e. $P_{\text{PHI}} \propto \Delta\sigma_{\text{scat}}$). Qualitatively, this arises because thermally-induced changes to specimen refractive indices change specimen scattering cross-sections.[32]

From Mie theory, the angular distribution of scattered light, $I_{\text{scat}}(r, n, \Theta)$,[32] is

$$I_{\text{scat}}(r, n, \Theta) = \sigma_{\text{scat}}(r, n, \Theta) \frac{P(r, n, \Theta)}{4\pi} I_0(\Theta, \phi) \tag{2}$$

where $P(r, n, \Theta)$ is the phase function (i.e. the ratio of energy scattered per solid angle in one direction to the total energy scattered per solid angle in all directions) and $I_0(\Theta, \phi)$ is the incident light intensity. Changes to I_{scat} (i.e. ΔI_{scat}) are therefore proportional to $\Delta\sigma_{\text{scat}}$, which, in turn, depends on changes to specimen refractive indices, size, and temperature as follows:

$$\Delta\sigma_{\text{scat}} = \left(\frac{\partial\sigma_{\text{scat}}}{\partial n} \frac{\partial n}{\partial T} + \frac{\partial\sigma_{\text{scat}}}{\partial r} \frac{\partial r}{\partial T} \right) \Delta T. \tag{3}$$

In **Equation 3**, $\frac{\partial n}{\partial T}$ is the specimen thermo-optic coefficient with $\frac{\partial r}{\partial T}$ its thermal expansion coefficient. What results is a predicted IR-PHI signal dependency that scales as

$$P_{\text{PHI}} \propto \Delta I_{\text{scat}} \propto \Delta\sigma_{\text{scat}}. \tag{4}$$

At this point, a characteristic feature of Mie scattering cross-sections is that they scale with sample geometrical area (i.e. $\propto \pi r^2$) for specimen sizes comparable to the wavelength of light.[32] Most impressive then

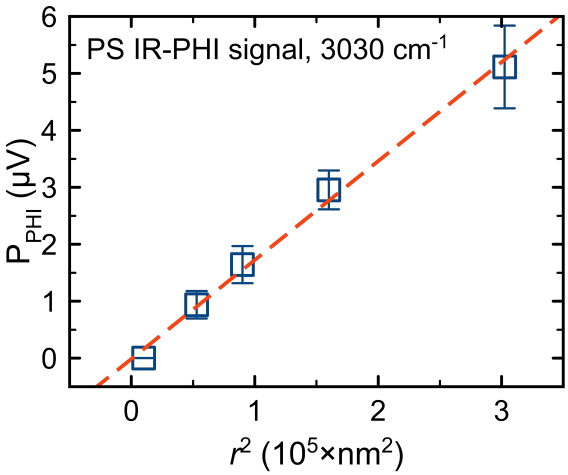

Figure 4: IR-PHI signal as a function of r^2. Square symbols represent experimental IR-PHI signals. The dashed line is a linear fit through the data.

is that **Figure 4** clearly shows this r^2 dependency. This, in turn, corroborates $\Delta\sigma_{\text{scat}}$ as the origin of IR-PHI signal contrast and links P_{PHI} to specimen physical parameters, namely, to $\frac{\partial n}{\partial T}$ and $\frac{\partial r}{\partial T}$ as well as size-dependent heat capacities and absorption cross-sections through **Equations 3** and **4**.

CONCLUSIONS

We have studied signal contrast in IR-PHI to place the technique on a more quantitative footing. Our analysis reveals that IR-PHI signal contrast originates from temperature-induced changes to specimen scattering cross sections. The analysis simultaneously links specimen material parameters to the PHI signal, suggesting future studies wherein IR-PHI can be used to quantitatively characterize material properties of isolated nanostructures in the all important MIR region of the spectrum.

ACKNOWLEDGMENTS

M.K. and G.V.H. acknowledge the National Science Foundation (grant numbers CHE-1563528 and CHE-1902403 respectively) for financial support. The IR OPO system was purchased through DURIP Award W911NF1410604. We thank the Notre Dame Energy Materials Characterization Facility (MCF) for use of its instrumentation. The MCF is funded by the Sustainable Energy Initiative (SEI), which is part of the Center for Sustainable Energy at Notre Dame (ND Energy).

REFERENCES

[1] Moerner, W. E. and Kador, L., "Optical detection and spectroscopy of single molecules in a solid," Phys. Rev. Lett. **62**, 2535 (1989).

[2] Orrit, M. and Bernard, J., "Single pentacene molecules detected by fluorescence excitation in a p-terphenyl crystal," Phys. Rev. Lett. **65**, 2716 (1990).

[3] Moerner, W. E. and Fromm, D. P., "Methods of single-molecule fluorescence spectroscopy and microscopy," Rev. Sci. Instrum. **74**, 3597 (2003).

[4] Chatterjee, R., Pavlovetc, I. M., Aleshire, K., and Kuno, M., "Single semiconductor nanostructure extinction spectroscopy," J. Phys. Chem. C **129**, 16443–16463 (2018).

[5] Silver, J. A., "Frequency-modulation spectroscopy for trace species detection: theory and comparison among experimental methods," Appl. Opt. **31**, 707–717 (1992).

[6] Carey, C. R., LeBel, T., Crisostomo, D., Giblin, J., Kuno, M., and Hartland, G. V., "Imaging and absolute extinction cross-section measurements of nanorods and nanowires through polarization modulation microscopy," J. Phys. Chem. C **114**, 16029–16036 (2010).

[7] Lo, S. S., Devadas, M. S., Majora, T. A., and Hartland, G. V., "Optical detection of single nano-objects by transient absorption microscopy," Analyst **138**, 25–31 (2013).

[8] Arbouet, A., Christofilos, D., Fatti, N. D., Vallée, F., Huntzinger, J. R., Arnaud, L., Billaud, P., and Broyer, M., "Direct measurement of the single-metal-cluster optical absorption," Phys. Rev. Lett. **93**, 127401 (2004).

[9] McDonald, M. P., Vietmeyer, F., Aleksiuk, D., and Kuno, M., "Supercontinuum spatial modulation spectroscopy: Detection and noise limitations," Rev. Sci. Instrum. **84**, 113104 (2013).

[10] Berciaud, S., Cognet, L., Blab, G. A., and Lounis, B., "Photothermal heterodyne imaging of individual nonfluorescent nanoclusters and nanocrystals," Phys. Rev. Lett. **93**, 257402 (2004).

[11] Berciaud, S., Lasne, D., Blab, G. A., Cognet, L., and Lounis, B., "Photothermal heterodyne imaging of individual metallic nanoparticles: Theory versus experiment," Phys. Rev. B **73**, 045424 (2006).

[12] Gaiduk, A., Ruijgrok, P. V., Yorulmaz, M., and Orrit, M., "Detection limits in photothermal microscopy," Chem. Sci. **1**, 343–350 (2010).

[13] Giblin, J., Syed, M., Banning, M. T., Kuno, M., and Hartland, G., "Experimental determination of single cdse nanowire absorption cross sections through photothermal imaging," ACS Nano **4**, 358–364 (2010).

[14] Whinnery, J. R., "Review of some photothermal effects," in [Amazing Light], Chiao, R. Y., ed., Springer, New York, NY (1996).

[15] Gaiduk, A., Yorulmaz, M., Ruijgrok, P. V., and Orrit, M., "Room-temperature detection of a single molecule's absorption by photothermal contrast," Science **330**, 353–356 (2010).

[16] Rice, J. H., "Nanoscale optical imaging by atomic force infrared microscopy," Nanoscale, 2010,2, 660-667 **2**, 660–667 (2010).

[17] Knoll, B. and Keilmann, F., "Near-field probing of vibrational absorption for chemical microscopy," Nature **399**, 134–137 (1999).

[18] Brehm, M., T.Taubner, Hillenbrand, R., and Keilmann, F., "Infrared spectroscopic mapping of single nanoparticles and viruses at nanoscale resolution," Nano Lett. 2006, 6, 7, 1307-1310 **6**, 1307–1310 (2006).

[19] Dazzi, A., Prazeres, R., Glotin, F., and Ortega, J. M., "Local infrared microspectroscopy with subwavelength spatial resolution with an atomic force microscope tip used as a photothermal sensor," Opt. Lett. **30**, 2388–2390 (2005).

[20] Hanson, K. M., "Introduction to Bayesian image analysis," in [Medical Imaging: Image Processing], Loew, M. H., ed., Proc. SPIE **1898**, 716–731 (1993).

[21] Lee, E. S. and Lee, J. Y., "Nonlinear optical infrared microscopy with chemical specificity," Appl. Phys. Lett. **94**, 261101 (2009).

[22] Mërtiri, A., Jeys, T., Liberman, V., Hong, M. K., Mertz, J., Altug, H., and Erramilli, S., "Mid-infrared photothermal heterodyne spectroscopy in a liquid crystal using a quantum cascade laser," Appl. Phys. Lett. **101**, 044101 (2012).

[23] Zhang, D., Li, C., Zhang, C., Slipchenko, M. N., Eakins, G., and Cheng, J.-X., "Depth-resolved mid-infrared photothermal imaging of living cells and organisms with submicrometer spatial resolution," Sci. Adv. **2**, e1600521 (2016).

[24] Totachawattana, A., Liu, H., Mertiri, A., Hong, M. K., Erramilli, S., and Sander, M. Y., "Vibrational mid-infrared photothermal spectroscopy using a fiber laser probe: asymptotic limit in signal-to-baseline contrast," Opt. Lett. **41**, 179–182 (2016).

[25] Li, C., Zhang, D. L., Slipchenko, M. N., and Cheng, J. X., "Mid-infrared photothermal imaging of active pharmaceutical ingredients at submicrometer spatial resolution," Anal. Chem. **89**, 4863– 4867 (2017).

[26] Li, Z., Aleshire, K., Kuno, M., and Hartland, G. V., "Super-resolution far-field infrared imaging by photothermal heterodyne imaging," J. Phys. Chem. B **121**, 8838–8846 (2017).

[27] Chatterjee, R., Pavlovetc, I. M., Aleshire, K., Hartland, G. V., and Kuno, M., "Subdiffraction infrared imaging of mixed cation perovskites: Probing local cation heterogeneities," ACS Energy Lett. **3**, 469–475 (2018).

[28] Samolis, P. D. and Sander, M. Y., "Phase-sensitive lock-in detection for high-contrast mid-infrared photothermal imaging with sub-diffraction limited resolution," Opt. Express **41**, 2643–2655 (2019).

[29] Bai, Y., Zhang, D., Lan, L., Huang, Y., Maize, K., Shakouri, A., and Cheng, J.-X., "Ultrafast chemical imaging by widefield photothermal sensing of infrared absorption," Sci. Adv. **5**, eaav7127 (2019).

[30] Lim, J. M., Park, C., Park, J.-S., Kim, C., Chon, B., and Cho, M., "Cytoplasmic protein imaging with mid-infrared photothermal microscopy: Cellular dynamics of live neurons and oligodendrocytes," J. Phys. Chem. Lett. **10**, 2857–2861 (2019).

[31] Halliday, D. and Resnick, R., [Fundamentals of Physics], Wiley (2013).

[32] Bohren, C. F. and Huffman, D. R., [Absorption and Scattering of Light by Small Particles], Wiley (1998).